Copyright ©2023 by the Magnetics Society of Japan.
This article is licensed under the Creative Commons Attribution International License (CC BY 4.0)
http://creativecommons.org/licenses/by/4.0/

J. Magn. Soc. Jpn., **47**, 90-102 (2023)

<Review>

First-principles Studies on Spin-dependent Transport of Magnetic Junctions with Half-metallic Heusler Compounds

Y. Miura*,**

*Research Center for Magnetic and Spintronic Materials (CMSM), National Institute for Materials Science (NIMS), *1-2-1 Sengen, Tsukuba, Ibaraki 305-0032, Japan*

**Center for Spintronics Research Network (CSRN), Graduate School of Engineering Science, Osaka University, *Machikaneyama 1-3, Toyonaka, Osaka 560-8531, Japan*

Two types of magnetoresistance (MR), i.e., tunnel magnetoresistance (TMR) and current perpendicular to plane giant magnetoresistance (CPP-GMR), are theoretically discussed for systems with half-metallic (HFM) Co-based full Heusler compounds. In TMR, the non-collinear spin structure at the Co_2MnSi(CMS)/MgO(001) interface that results from thermal spin fluctuations significantly reduced the TMR ratio at room temperature (RT). Enhancement of the exchange stiffness of CMS/MgO was essential to suppress the reduction in TMR at RT. Furthermore, it is proposed that inserting of a B2-CoFe layer between CMS and MgO is a promising way to enhance the interface exchange stiffness constant. In CPP-GMR, the interface spin asymmetry γ in the Valet-Fert model was essential to enhance GMR at RT, because the temperature dependence of γ in experiments was much larger than that of the bulk spin asymmetry ß. I showed that the experimental CPP-GMR ratio increases with the decrease in the theoretical resistance-area product R_PA, which is roughly consistent with the R_P dependence of γ. This means that matching of the conductive channel between HMF and a non-magnetic metallic spacer is a key parameter to enhance γ. These findings will be very important for room temperature spintronics devices applied in future artificial intelligence hardware.

Key words: magnetoresistance, first-principles calculation, Heusler compound, TMR, CPP-GMR, ballistic transport, exchange stiffness

1. Introduction

I introduce "Theoretical Study on Spin-dependent Transport Properties in Magnetic Junctions" in this review paper, which was a research subject of MSJ Outstanding Research Award 2022.

The spin-dependent tunneling between two ferromagnetic (FM) electrodes separated by a non-magnetic (NM) layer provides magnetoresistance (MR) that depends on the relative magnetization directions of the ferromagnetic electrodes.[1–3] The effect is applied in magnetoresistive random access memory (MRAM) and ultra-sensitive magnetoresistive sensors, which are essential to realize artificial intelligence (AI) hardware and neuromorphic devices in the next-generation information society.[4,5] There are two types of MR devices according to the type of nonmagnetic layer, which are tunneling magnetoresistance (TMR) devices with an insulating barrier layer, and current-perpendicular-to-plane giant magnetoresistance (CPP-GMR) devices with a NM metal spacer. To realize AI-dedicated and neuromorphic spintronics devices, a large MR ratio and low resistance are required.

High TMR ratios over 300% at room temperature have been realized in magnetic tunnel junctions (MTJs) with single-crystalline MgO and bcc-FeCo[6–8] from coherent tunneling through the Δ_1 evanescent state in MgO and the highly spin-polarized Δ_1 band around the Fermi level in bcc-FeCo[9,10]. This means that in TMR devices, the spin dependence of the current can be characterized by the spin polarization of the Δ_1 state of the ferromagnetic electrodes at in-plane wave vector $\mathbf{k}_\parallel = \mathbf{0}$ rather than that of the total density of states (DOSs) around the Fermi level. In MgO-based MTJs, it is difficult to reduce the resistance while maintaining high TMR. Reducing the barrier thickness of MTJs decreases the TMR as well as the resistance, because the tunneling of non-spin-polarized Δ_5 and Δ_2 states is not negligible in a MgO layer with a thickness of a few monolayers. Thus, half-metallic ferromagnets (HMFs), which are metallic for the majority-spin band and insulating for the minority-spin band with complete (100%) spin polarization at the Fermi level, will be important to realize both high TMR and low resistance for MTJs with few-monolayer MgO thickness.

CPP-GMR devices composed of all-metallic layers have lower resistance than TMR devices, but their MR ratios are also typically more than an order of magnitude smaller. This is due to the presence of many scattering processes in all-metallic systems, because in a metallic system, not only electrons with $\mathbf{k}_\parallel = \mathbf{0}$ but also those with $\mathbf{k}_\parallel \neq \mathbf{0}$ contribute equally to the current. Thus, the spin-dependent transport in GMR devices can be characterized by the spin polarization of the total DOSs of the ferromagnetic electrodes rather than the spin polarization at the specific $\mathbf{k}_\parallel$, and HMFs again are

Corresponding author: Y. Miura
(e-mail: MIURA.Yoshio@nims.go.jp)

Table 1 Summary of experimental results on TMR ratio [%] at room temperature (RT) and low temperature (LT) for MTJs with Co-based full Heusler compounds Co_2YZ (exact temperatures differ between studies).

Bottom electrode	Barrier	Upper electrode	TMR % @ LT	TMR % @ RT	Year [Reference]
$Co_2(Cr_{0.6}Fe_{0.4})Al$	Al-O	$Co_2(Cr_{0.6}Fe_{0.4})Al$	26.5	16	2003[26]
Co_2MnAl	Al-O	$Co_{0.5}Fe_{0.5}$	40	27	2004[27]
Co_2FeAl	Al-O	$Co_{0.75}Fe_{0.25}$		47.3	2005[28]
Co_2MnSi	Al-O	Co_2MnSi	570	67	2006[29]
$Co_2Fe(Al_{0.5}Si_{0.5})$	Al-O	$Co_{0.75}Fe_{0.25}$	106	76	2006[30]
$Co_2(Cr_{0.6}Fe_{0.4})Al$	MgO	$Co_{0.5}Fe_{0.5}$	240	90	2007[31]
Co_2MnSi	MgO	$Co_{0.5}Fe_{0.5}$	753	217	2008[32]
Co_2MnSi	MgO	Co_2MnSi	700	180	2009[33]
$Co_2Fe(Al_{0.5}Si_{0.5})$	MgO	$Co_2Fe(Al_{0.5}Si_{0.5})$	832	386	2009[34]
Co_2FeAl	MgO	Co_2FeAl	308	130	2009[35]
Co_2FeAl	MgO	CoFe	700	330	2010[36]
$Co_2Mn_{1.29}Si$	MgO	$Co_2Mn_{1.29}Si$	1995	354	2012[37]
$Co_2(Fe_{0.5}Mn_{0.5})Si$	MgO	$Co_2(Fe_{0.5}Mn_{0.5})Si$	2610	429	2015[38]
Co_2FeAl	$MgAl_2O_4$	$Co_2Fe(Al_{0.5}Si_{0.5})$	616	342	2016[39]
$Co_2Mn_{1.3}Si_{0.84}$	MgO	$Co_2Mn_{1.3}Si_{0.84}$	2010	335	2016[40]
$Co_2Fe(Ga_{0.5}Ge_{0.5})$	$Cu(In_{0.8}Ga_{0.2})Se_2$	$Co_2Fe(Ga_{0.5}Ge_{0.5})$	100	40	2016[41]
$Co_2Fe(G_{a0.5}Ge_{0.5})$	$CuGaSe_2$	$Co_2FeGa_{(0.5}Ge_{0.5})$	250	100	2019[42]

important for obtaining large GMR.

Among the many theoretically predicted HMFs,[11–16] the Co-based full Heusler compounds Co_2YZ (Y = Cr, Mn, Fe, Z = Al, Si, Ga, Ge) are the most promising candidates for use in spintronics devices because of their high Curie temperatures above room temperature (RT). A characteristic feature of Co-based full Heusler compounds is that their electronic structure hardly changes with respect to the specific atomic disorder, such as B2-type disorder, where Y and Z atom sites are randomly occupied.[17–19] The robustness of high spin polarization against the atomic disorder of Co-based Heusler compounds is important in terms of the relaxation of experimental requirements, because it is expected that some degree of atomic disorder will occur during thin-film fabrication. The valence-band electronic structures of typical halfmetallic Co-based full Heusler compounds Co_2MnSi (CMS) were investigated by photoelectron spectroscopy to confirm the temperature dependence of the electronic structures.[20] The experimental valence band photoemission spectra at 30 K were in good agreement with density functional theory (DFT) calculations at zero temperature, and no distinct temperature dependence was observed in the experimental valence band spectra. Furthermore, the temperature dependence of the spin-polarization of CMS was shown to be small by spin-resolved hard x-ray photoelectron spectroscopy.[21] Recently, we calculated the temperature dependence of the bulk electronic structures of half-metallic Co-based Heusler compounds using the disordered local moment (DLM) method,[22] and found that the temperature dependence of the spin-polarization of the *sp* density of states (DOS) of $Co_2FeGa_{0.5}Ge_{0.5}$ (CFGG) is weaker than that of CMS.[23,24] Furthermore, several new Co-based Heusler compounds such as $Co_2MnGa_{1-x}As_x$ and $Co_2FeAl_{1-x}Sn_x$ were proposed by the machine learning method with finite temperature first-principles calculations using the DLM.[25]

Table 1 summarizes experimental studies on TMR ratios at low temperature (LT) and RT for Co-based full Heusler MTJs[26-42]. Half-metallic Co_2YZ compounds have been applied in TMR devices with an amorphous alumina barrier[26–30] and then in MTJs with a MgO barrier, and large TMR ratios were demonstrated.[31–38,40] Furthermore, new barrier materials such as $MgAl_2O_4$[39] and $Cu(In_{1-x}Ga_x)Se_2$[41,42] have been applied as the barrier layer in Heusler-based MTJs. Particularly, MTJs with Mn-rich CMS and $Co_2(Mn,Fe)_aSi$ with MgO barriers provided huge TMR exceeding 2000% at very low temperature,[38,40] indicating the potential of the halfmetallic electronic structures. However, the TMR also rapidly decreases with increasing temperature.

As is shown in Table 1, experiments on the TMR effect of MTJs with half-metallic Co-based full Heusler compounds have not been reported after 2019. There are two reasons for the decrease in experimental studies on TMR in Heusler-based MTJs. One is the large temperature dependence of the TMR ratios of MTJs with half-metallic Co-based full Heusler compounds.

Table 2 Summary of experimental results on GMR ratio % and ΔRA mΩ · μm² at room temperature (RT) and low temperature (LT) for CPP-GMR devices with Co_2YZ (exact temperatures differ between studies).

System	GMR % @ LT (ΔRA mΩ · μm²)	GMR % @ RT (ΔRA mΩ · μm²)	Year [Reference]
Co_2MnSi/Cr/Co_2MnSi(001)		2.4 (19)	2006[49]
Co_2MnSi/Cu/Co_2MnSi(001)		9	2008[50]
$Co_2Fe(Al_{0.5}Si_{0.5})$/Ag/$Co_2Fe(Al_{0.5}Si_{0.5})$(001)	14 (12.4)	6.9 (7.4)	2008[51]
Co_2MnSi/Cr/Co_2MnSi(001)		5.2 (6.5)	2009[52]
Co_2MnSi/Ag/Co_2MnSi(001)		28.8 (8.92)	2009[53]
$Co_2Fe(Al_{0.5}Si_{0.5})$/Ag/$Co_2Fe(Al_{0.5}Si_{0.5})$(001)	80 (17)	34 (8)	2010[54]
$Co_2Mn(Ga_{0.5}Sn_{0.5})$/Ag/$Co_2Mn(Ga_{0.5}Sn_{0.5})$(001)	17.2 (6.5)	8.8 (4)	2010[55]
Co_2MnSi/Ag/Co_2MnSi(001)	67.2	36.4 (11.5)	2010[56]
$Co_2Fe(Ga_{0.5}Ge_{0.5})$/Ag/$Co_2Fe(Ga_{0.5}Ge_{0.5})$(001)	129.1 (26.4)	41.7 (9.5)	2011[57]
Co_2MnGe/Cu/Co_2MnGe(001)		9 (6)	2011[58]
$Co_2(Fe_{0.4}Mn_{0.6})Si$/Ag/$Co_2(Fe_{0.4}Mn_{0.6})Si$(001)		74.8	2011[59]
$Co_2(Fe_{0.4}Mn_{0.6})Si$/Ag/$Co_2(Fe_{0.4}Mn_{0.6})Si$(001)	184	58 (11)	2012[60]
$Co_2Fe(Ga_{0.5}Ge_{0.5})$/Ag/$Co_2Fe(Ga_{0.5}Ge_{0.5})$(001)	183 (33)	57 (12)	2013[61]
$Co_2Fe(Ga_{0.5}Ge_{0.5})$/NiAl/Ag/NiAl /$Co_2Fe(Ga_{0.5}Ge_{0.5})$(001)	285 (78)	82 (31)	2016[62]
$Co_2Mn_{1.45}Si_{0.82}$/CoFe/Ag/CoFe/$Co_2Mn_{1.45}Si_{0.82}$(001)		20.7 (3.1)	2017[63]
$Co_2(Fe_{0.4}Mn_{0.6})Si$/Ag_3Mg/$Co_2(Fe_{0.4}Mn_{0.6})Si$(001)		63 (25)	2017[64]
$Co_2(Fe_{0.4}Mn_{0.6})Ge$/AgSn/$Co_2(Fe_{0.4}Mn_{0.6})Ge$(001)		25 (7.5)	2018[65]
$Co_2(Fe_{0.4}Mn_{0.6})Si$/Ag_3Mg/$Co_2(Fe_{0.4}Mn_{0.6})Si$(001)	100	30	2019[66]
$Co_2Fe(Ga_{0.5}Ge_{0.5})$/Ni/Ag/Ni/$Co_2Fe(Ga_{0.5}Ge_{0.5})$(001)		32.5	2021[67]
CoFe/$Co_2(Fe_{0.4}Mn_{0.6})Si$/Ag/$Co_2(Fe_{0.4}Mn_{0.6})Si$/CoFe(001)		50 (19.1)	2021[68]

The TMR ratio of Heusler-based MTJs at RT is still smaller than that of CoFe-based MTJs. Recently, a breakthrough in the RT TMR of CoFe-based MTJs was achieved by Scheike *et al.*, where a 631% TMR ratio at RT and 1143% TMR ratio at LT were observed for CoFe/MgO/CoFe(001) MTJs.[43] To demonstrate the potential of half-metallic Heusler compounds, it is important to achieve a larger TMR ratio at RT than that of CoFe-based MTJs. The other reason for the decrease in studies is requirement of MTJs with the perpendicular magnetic anisotropy (PMA). In spin-transfer torque switching of the magnetization direction in MTJs, PMA is required in order to reduce the effective anisotropy field of MTJs. Since the Co-based full Heusler compounds show basically cubic symmetry, the magneto-crystalline anisotropy (MCA) of Co_2YZ is zero. Thus, the magnetic anisotropy of Co_2YZ(001) thin films tends to have an in-plane easy axis due to the shape anisotropy. Some Mn-based Heusler compounds such as Mn_3Ga and Mn_3Ge with $D0_{22}$ structure have tetragonal structures, showing perpendicular MCA in the bulk.[44–47] However, the experimental results for the TMR effects of Mn_3Ga/MgO- and Mn_3Ge/MgO-based MTJs[44,48] are very small compared with those of Co_2YZ/MgO-based MTJs because of the large lattice mismatch of Mn_3Ga and Mn_3Ge with MgO[47] and the non-half-metallic behavior of the Δ_1 states of Mn_3Ga.[44] Therefore, achieving perpendicular MCA in Heusler-based MTJs will be also a future task.

Table 2 summarizes experimental studies on GMR ratios and the difference in resistance-area product between parallel and antiparallel magnetizations ΔRA at LT and RT for various CPP-GMR systems with Co-based full Heusler compounds.[49-68] Half-metallic Co_2YZ have also been applied in CPP-GMR devices, and relatively large GMR ratios have been observed for Heusler-based magnetic junctions with a Cr spacer,[49,52] Cu spacer,[50,58] Ag spacer,[51,53–57,59–61] Ag_3Mg spacer[64,66] and AgSn spacer.[65] Furthermore, insertions of an additional layer were attempted to enhance the matching of conductive channels between Co-based full Heusler compounds and NM spacers, such as NiAl insertion in the CFGG/Ag(001) interface,[62] Ni insertion in the CFGG/Ag(001) interface,[67] CoFe insertion in the CMS/Ag(001) interface[63] and $Co_2(Fe_{0.4}Mn_{0.6})Si$ insertion in the CoFe/Ag(001) interface,[68] which led to an increase in the CPP-GMR ratios.

In this review, I discuss the spin-dependent transport properties of TMR and CPP-GMR devices with half-metallic Co_2YZ based on first-principles electronic structure and ballistic transport calculations. Particularly, I focus on the spin-dependent transport of magnetic junctions with half-metallic Co_2YZ. First, I discuss the origin of the temperature dependence of the TMR ratios in MTJs. The spin-dependent conductance

of MTJs with CMS (or Fe) and MgO was investigated based on first-principles calculations in a noncollinear spin system. Noncollinear magnetic structures are formed as a result of spin fluctuation at finite temperatures. I focus on the spin-flip scattering of conducting electrons caused by the noncollinearity of local spin moments in various interfacial layers, and I discuss the electronic states at the interfaces that contribute to the spin-flip conductance. Our theoretical analysis confirmed the crucial contribution of the spin-flip process at the interface, which leads to a significant reduction in the MR ratio at RT. Then, I discuss the interface spin-asymmetry in CPP-GMR devices. I argue that the matching of the Fermi surface projected to the two-dimensional Brillouin zone in in-plane wave vector $\mathbf{k}_{\parallel}$ between the CMS and NM spacers is important to enhance the interface spin asymmetry. Furthermore, I clarify the correlation between experimental CPP-GMR ratios and the theoretical interface resistance in parallel magnetization in CPP-GMR.

2. Computational Method

I performed first-principles calculations for supercells consisting of Co-based Heusler compounds Co_2YZ (Y = Mn or Fe, Z = Si, Ga or Ge) and various non-magnetic (NM) layers X such as X = MgO, Ag, Cr, V, Al and Au using the DFT within the generalized-gradient approximation for the exchange-correlation energy.[69] In order to facilitate the optimization of atomic positions, which is important for determining the interface structure, I adopted plane-wave basis sets along with the ultra-soft pseudopotential method by using the quantum code ESPRESSO.[70] The number of k points is taken to be 15×15×1 for all cases, and Methfessel-Paxton smearing with a broadening parameter of 0.01 Ry is used. The cutoff energy for the wavefunction and charge density is set to 30 Ry and 300 Ry, respectively. These values are large enough to deal with all the elements considered here within the ultra-soft pseudopotential method. $Co_2YZ/X/Co_2YZ(001)$ magnetic junctions with Co (YZ) termination were constructed in a multilayer structure containing seventeen (fifteen) atomic layers of Co_2YZ and seven or nine atomic layers of NM. The in-plane lattice parameter of the supercell is fixed to that of Co_2YZ. These values correspond to $a_0/\sqrt{2}$, where a_0 is the lattice constant of the bulk Co_2MnSi (5.65 Å). Since the lattice constant of the NM layer X is different from that of Co_2YZ, the lattice mismatches between Co_2YZ and X on the 45° in-plane rotation at the (001) face are considered, leading to tetragonal distortion in the NM layer (X).

For transport calculations, I calculated the ballistic conductance of the magnetic junctions based on the Landauer formula.[71] I considered an open quantum system consisting of a scattering region corresponding to NM spacer X and a junction with Co_2YZ attached to left and right semi-infinite electrodes corresponding to bulk Co_2YZ. The transmittance can be obtained by solving the scattering equation with infinite boundary conditions, in which the wavefunction of the scattering region and its derivative are connected to the Bloch states of each electrode.[72] The potential in the scattering equation can be obtained from self-consistent filed electronic structure calculations for the supercell containing a left electrode and a scattering region. It was confirmed that five atomic layers of Co_2YZ between the right edge of the electrode region and the left-hand side of the Co_2YZ/X interface are sufficient to represent the shape of the local potential of bulk Co_2YZ in the electrode region.

Since our system is repeated periodically in the xy plane and propagating states can be assigned by an in-plane wave vector $\mathbf{k}_{\parallel} = (k_x, k_y)$ index, different $\mathbf{k}_{\parallel}$ do not mix and can be treated separately. Furthermore, our approach neglects the spin-orbit interaction and noncollinear spin configuration. Thus, I solved scattering equations for some fixed $\mathbf{k}_{\parallel}$ and spin index using Choi and Ihm's method.[72, 73]

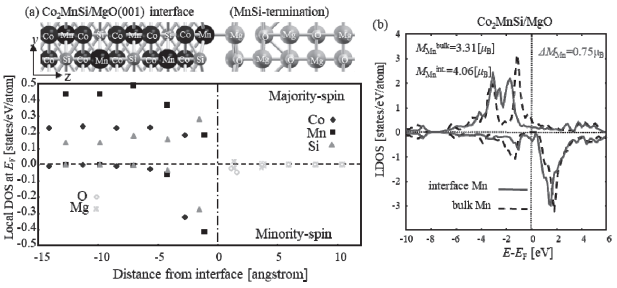

Fig. 1 Local density of states (LDOS) at Fermi level (E_F) projected onto each atomic sphere as a function of the distance from interface for Co_2MnSi(CMS) /MgO(001) with MnSi termination. Positive (negative) sign of y-axis indicates majority-spin (minority-spin) LDOS. Schematic figures of supercell of CMS/MgO/CMS(001) MTJ are shown above the LDOS. (b) The solid lines show LDOS of Mn d at MnSi-terminated CMS/MgO(001) interface as a function of energy relative to E_F. LDOS in bulk (electrode) region is also shown by dashed line as a reference. ref.[74]

3. Spin-dependent transport in TMR devices

3.1 Interface electronic structures

Figure 1(a) shows the majority- and minority-spin local density of states (LDOS) at the Fermi level projected onto each atomic sphere as a function of the distance from the Co_2MnSi(CMS)/MgO(001) junction.[74] It is found that in the case of MnSi termination, interface states appear in the minority-spin state at the Fermi level, reducing the half-metallicity of CMS. Similar results have been obtained in the Co termination of the CMS/MgO(001) junction.[75] Examining the electronic structure at the interface in

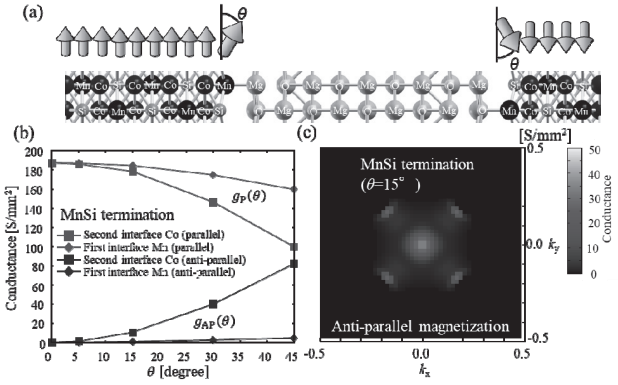

Fig. 2 (a) Schematic figure of CMS/MgO/CMS MTJs with MnSi termination and local spin moments for each layer, with a noncollinear magnetic structure on both sides of junction. (b) Parallel and antiparallel conductance of CMS/MgO/CMS MTJ as a function of the angle of interfacial local spin moments θ. (c) In-plane wave-vector (**k**∥) dependence of antiparallel conductance of CMS/MgO/CMS MTJ with θ = 15° for MgO thickness ~ 2.0 nm (nine atomic layers of MgO). ref. [81]

more detail, Fig. 1(b) presents the majority- and minority-spin LDOS of each atom and atomic orbital in the MnSi-terminated CMS/MgO(001). The LDOS in the bulk (electrode) region is also shown as a reference. In Fig. 1(b), it is found that the spin moment of the interfacial Mn (4.06 μ_B) is larger than those of the bulk CMS (3.31 μ_B) due to the charge transfer from the minority-spin to the majority-spin states. I considered that the relaxation of the atomic positions and the reduced symmetry at the interface cause charge transfer from the minority-spin to the majority-spin 3*d* states owing to the localization effect of 3*d* electrons.

Furthermore, in Fig. 1(b), minority-spin states are observed around the Fermi level in the LDOS of the interfacial Mn and Si atoms. The spin polarizations of interface Mn and Si are -0.4 and 0.01, respectively. At the interface, the Mn atom loses half of its first nearest neighbor Co atoms, and non-bonding Mn *d* states (possibly d_{yz}, d_{zx} and $d_{3z^2-r^2}$) can appear around the Fermi level. Since the Mn $d_{3z^2-r^2}$ orbital hybridizes with the O p_z orbital at the interface, the LDOS of the interfacial Mn d_γ states maintain a half-metallic character. Contrary to this, the interfacial Mn d_ε orbitals (d_{yz} and d_{zx}) become nonbonding in the O-top configuration, reducing the spin polarization at the MnSi termination. Mavropoulos, *et al.* suggested that the interface states that appear in the minority-spin gap at the junctions of MTJs can also contribute to the tunneling conductance in anti-parallel magnetization, through spin mixing processes such as magnon excitations and inelastic scattering at RT.[76-78]

3.2 Spin-flip scattering at interfaces

Since the CMS/MgO(001) interface is not half-metallic

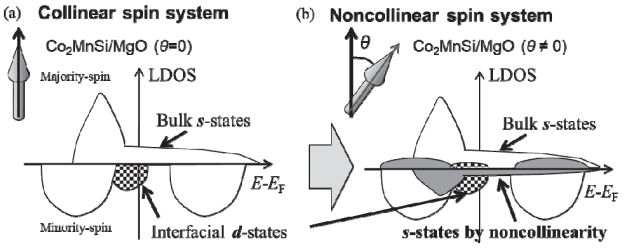

Fig. 3 Schematic images of LDOS for interface Co or Mn atoms of CMS in (a) collinear spin system (θ = 0) and (b) noncollinear spin system (θ ≠ 0), respectively. Gray areas and cross-hatched black areas indicate the interface *d*-states and interface *s*-states, respectively. ref. [81]

due to the appearance of non-bonding states in the minority-spin states around the Fermi level, the spin-flip scattering can be enhanced at finite temperature through the interface states as a result of the thermal fluctuation of magnetic spin moments.[79] Thus, the effects of thermal fluctuation and the noncollinear magnetic structure at the interface of MTJ on the spin-dependent transport are considered. The potential for a noncollinear-spin system was obtained by rotating the density matrix of a collinear-spin system with a spin-1/2 rotation matrix. According to Kübler's formulation,[79,80] off-diagonal elements of the effective potential that provide spin-mixing in the ballistic conductance are given by

$$(\delta E_{xc}/\delta n_\uparrow - \delta E_{xc}/\delta n_\downarrow)(\sin\theta\cos\varphi \pm i\sin\theta\sin\varphi)/2, \quad (1)$$

where $\delta E_{xc}/\delta n_s$ ($s = \uparrow, \downarrow$) is the exchange and correlation potential in a collinear-spin system and θ and φ are the polar and azimuthal angles of a local spin moment with respect to the global spin-quantum axis, respectively. Since our calculations neglected spin-orbit interaction, the azimuthal angle φ did not affect the calculation results and was set to zero. The off-diagonal part of the local potential expressed by equation (1) is given at real-space positions of the supercell within each atomic sphere of interfacial atoms having a noncollinear spin moment.

Fig. 2 (a) shows the model system used for CMS/MgO/CMS MTJs with MnSi termination in the anti-parallel magnetization, where the interface Mn and sub-interface Co spin moments on both sides of the junction were canted by an angle θ in order to provide interfacial spin-flip scattering.[81] Figure 2(b) shows the conductance of a CMS/MgO/CMS MTJ with MnSi termination in parallel or anti-parallel magnetization as a function of the angle of the interface spin moments. zero conductance was obtained at θ = 0° for anti-parallel magnetization because of the half-metallic character of CMS. On the other hand, the anti-parallel conductance increased with increasing θ, while the parallel conductance decreased. This behavior can be attributed to spin-flip scattering because of the noncollinear interfacial magnetic structures. Fig. 2(c) shows the in-plane wave-vector (**k**∥) dependence of the tunneling conductance of the MTJ in anti-parallel magnetization with the interfacial Mn spin moment θ = 5°. It was already shown in ref. [74,75] that bulk CMS has a Δ_1 band at the Fermi level in the majority-spin states, and

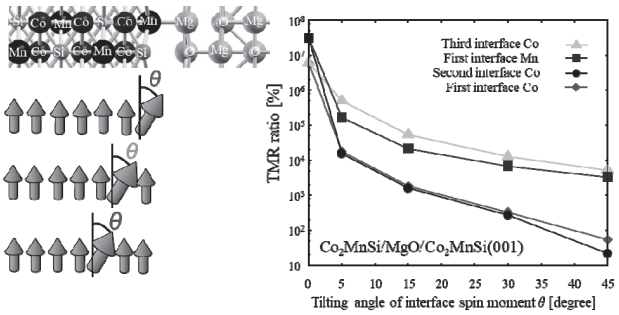

Fig. 4 Logarithmic plots of TMR ratios as a function of angle of local spin moment θ for noncollinear magnetic structures of various interfacial layers in CMS/MgO/CMS MTJs and Fe/MgO/Fe MTJs. ref. [81]

the $\mathbf{k}_{\parallel}$-dependence of the conductance of CMS/MgO/CMS MTJs in parallel magnetization has a broad peak at $\mathbf{k}_{\parallel} = (0,0)$ because of the slow decay of Δ_1 states in the MgO barrier.[9] As can be seen in Fig. 2(c), the $\mathbf{k}_{\parallel}$-dependence of the conductance in anti-parallel magnetization also shows a broad peak at $\mathbf{k}_{\parallel} = (0,0)$, indicating that the spin-flip conductance is dominated by the Δ_1 channel of the conducting electrons.

Fig. 3 shows schematic images of the LDOS of interface Mn and sub-interface Co atoms in collinear spin ($\theta = 0^\circ$) and noncollinear spin ($\theta \neq 0^\circ$) cases.[81] In the case of a collinear spin system, the CMS/MgO interface is not half-metallic and has interface states in the half-metallic gap of minority-spin states originating from the non-bonding Mn *d* orbital (see also Fig. 3 in ref. [75]). Then, the noncollinear spin moments of interface Mn and Co generate spin-mixing in the LDOS of CMS/MgO/CMS(001). At the Fermi level, as shown in Fig. 3(b), both bulk *s*-states and interfacial Mn *d*-states are projected on the majority-spin and minority-spin states of the global spin-quantum axis, providing spin-flip scattering of the Ballistic conductance. The broad peak at $\mathbf{k}_{\parallel} = (0,0)$ in Fig. 3(c) indicates that the projected minority-spin Δ_1 states mainly contribute to the conductance in anti-parallel magnetization. This means that the contribution of the interfacial d-states that appeared at the MnSi termination of CMS/MgO junctions in the collinear-spin system (cross-hatched black areas in Fig. 3(a) and (b)) was rather small compared to that of the *s*-states caused by the noncollinearity of interfacial Mn and Co spin moments (light-gray areas in Fig. 3(b)). Since the interface states were mainly composed of d_{xy} and $d_{x^2-y^2}$ orbitals of interfacial Mn and Co atoms, they show fast decay in the MgO barrier.

3.3 Effects of noncollinear magnetism on TMR

To examine the interfacial structure dependence of the spin-flip conductance, Fig. 4 shows logarithmic plots of TMR ratios as a function of the angle of the local spin moment θ in various interfacial layers of CMS/MgO/CMS. First, I can confirm that the TMR ratios of the MTJs decreased with increasing θ due to the spin-flip conductance in the interfacial region. In particular, the TMR ratios for CMS/MgO/CMS MTJs with noncollinear first and second interface Co spin moments had values similar to that of Fe/MgO/Fe MTJs for $\theta > 5^\circ$. This indicates that the advantage of half-metallic electrodes is valid only for small θ if the noncollinearity arises at interfacial Co spin moments. On the other hand, the decrease in the TMR ratio with increasing θ was rather gradual for MTJs with noncollinearity in the first interface Mn spin moment at the MnSi termination and the third interface Co spin moment, compared to that in the first and second Co layers, indicating that the spin-flip conductance was suppressed at the interfacial MnSi-layers and that spin-flip scattering mainly occurred in the first and second Co layers. Since the Si atom is nonmagnetic, the off-diagonal part of the effective potential expressed by $(\delta E_{xc}/\delta n_{\uparrow} - \delta E_{xc}/\delta n_{\downarrow})$ was rather small, which led to a suppression of the spin-flip probability at the MnSi-layer. In the calculations, the angle dependence of the size of the Co and Mn spin moments was neglected. This is a reasonable approximation for Mn spin moments in view of their localized character in bulk CMS[82,83] and MnSi-terminated interfaces.[84] For Co-terminated interfaces, the strong hybridization between Co and O atoms can cause angular dependence for the interfacial Co spin moments. As discussed for Ni spin moments in NiMnSb,[85] longitudinal fluctuations will increase the length of the local spin moments with increasing angle. This will enhance spin-flip scattering in interfacial regions, resulting in further decrease in the TMR ratio.

3.4 Exchange stiffness at interfaces

To estimate the exchange stiffness of the interfacial spin moments, The increase in the one-electron band energy $E(\theta)$ relative to the collinear-spin system ($\theta = 0^\circ$) was calculated. Fig. 5(a) shows $E(\theta)$ as a function of the angle of local moments θ for various interfacial layers in CMS/MgO(001) and Fe/MgO(001) junctions.[81] Then, the results were fitted using $E(\theta) = B(1-\cos\theta)$. Here, B is the inter-atomic-layer exchange stiffness constant; the value in Table 3 for each layer in the interfacial and bulk regions is shown in Table 3. This estimation corresponds to the magnetic force theorem method.[86,87]

It was confirmed that the increase in the band energy as a function of the canting angle shown in Fig. 5(a) can be fitted by $\sim \theta^2$ up to $\theta = 30^\circ$. This means that the error in the estimation of the exchange stiffness constant by the magnetic force theorem is very small in the present system.[88] First, it can be found that the exchange stiffness of the interfacial Co layer at the Co termination was much smaller than that of the interfacial MnSi-layer at the MnSi termination and that of bulk CMS. These results are consistent with the results of recent first-principles calculations of the exchange constant of CMS/MgO(001).[89]

Furthermore, the exchange stiffness of the

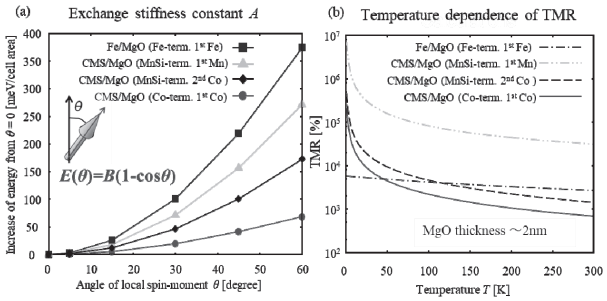

Fig. 5 (a) Increase in band energy relative to that of collinear-spin system $E(\theta)$ as a function of angle of local spin moments θ for first-layer Co spin moment at Co termination, first-layer Mn spin moment and second-layer Co spin moment of CMS/MgO(001), and first-layer Fe spin moment of Fe/MgO(001) junctions. ref. [81] (b) Temperature dependence of TMR ratios of CMS/MgO/CMS(001) and Fe/MgO/Fe(001) calculated by Eq. (2) including noncollinear spin structure of various spin moments.

sub-interfacial Co-layer at the MnSi termination was smaller than that of the interfacial MnSi-layer. This means that at the MnSi termination, the sub-interfacial Co spin moments fluctuate more easily than interfacial Mn spin moments. On the other hand, a very high exchange stiffness was found for the interfacial Fe-layer at Fe/MgO junctions compared to those of CMS/MgO junctions, indicating the robustness of interfacial Fe spin moments against thermal fluctuation. One possible reason for this behavior of the exchange stiffness in interfacial regions compared to that of bulk CMS is related to the change in the interfacial spin moments.

As is discussed in ref. [75,84] the majority-spin charge of interfacial Co atoms transfers to the MgO side because of the strong bonding between Co and O atoms. On the other hand, the interfacial Mn spin moments of the CMS/MgO junction[74,84] and interfacial Fe spin moments of the Fe/MgO junction[9,81] increase in comparison with those of the bulk because of the localization effect (and band-narrowing effect) of the non-bonding *d*-orbitals in the interfacial regions. Since $E(\theta)$ can be characterized by the off-diagonal elements of the local potential expressed by equation (1), the decrease (increase) of local spin moments reduced (enhanced) the off-diagonal terms, leading to the low (high) exchange stiffness.

3.5 Temperature dependence of TMR

Finally, I discuss the effect of interfacial spin-flip scattering on the TMR ratios at finite temperatures. To estimate the TMR ratio at a finite temperature, the Boltzmann average of the tunneling conductance was calculated using the following equation,

$$G_{P(AP)}(\theta) = \int g_{P(AP)}(\theta) \exp(-2E(\theta) / k_B T) \sin\theta \, d\theta \Big/ \int \exp(-2E(\theta) / k_B T) \sin\theta \, d\theta, \quad (2)$$

where $g_{P(AP)}(\theta)$ is the θ-dependence of the tunneling conductance in parallel (P) and anti-parallel (AP) magnetization, as shown in Fig. 2(b). $E(\theta)$ is the increase in the band energy caused by the noncollinearity of the local spin moments at each interfacial layer, as discussed in the previous paragraph. The factor of 2 for $E(\theta)$ indicates contribution from both sides of the MTJs.

Fig. 5(b) shows the calculated temperature dependence of the TMR ratio for the MTJs of CMS/MgO/CMS and Fe/MgO/Fe MTJs with 2 nm MgO thickness. As can be seen here, the reduction in the TMR ratios of CMS/MgO/CMS MTJs with the 1st layer Co spin fluctuation at Co termination and the 2nd layer Co spin fluctuation at MnSi termination are much faster than that of Fe/MgO/Fe MTJs with 1st layer Fe spin fluctuation. This means that the interfacial spin-flip scattering significantly reduces the TMR ratio at RT.

This result qualitatively agrees with the results of the temperature dependence of the TMR ratio. The temperature dependence of the TMR ratios of CMS/MgO/CMS MTJs with the 1st layer Mn spin fluctuation at the MnSi termination is also significant, but the TMR ratio maintains a large value at RT, indicating that the large exchange stiffness constant at the interface improves the TMR ratio at RT. The tunneling conductance evaluated at finite temperature using equation (2) is 700% at RT for CMS/MgO/CMS MTJs with the thermal fluctuation of the first layer Co spin moment at the Co termination, and 1500% at RT with the thermal fluctuation of the 2nd Co spin moment at the MnSi termination. These TMR ratios are smaller than the TMR ratio of 2500% at 300 K for Fe/MgO/Fe MTJs with thermal fluctuation of the 1st layer Fe spin moment.

From these results, I can conclude that the experimentally observed low TMR ratio of the MTJs at RT can be attributed to the spin-flip conductance caused by thermal fluctuation of the interfacial spin moments. Therefore, to suppress the reduction of the TMR ratios at finite temperature in CMS/MgO/CMS MTJs, the exchange stiffness of Co spin moments at the CMS/MgO(001) interface must be enhanced. In estimating the thermal average of the tunneling conductance, $E(\theta)$ was treated as the thermal excitation energy of the local spin moments per in-plane unit cell area, which corresponds to the replacement of various

Table 3 Inter-layer exchange stiffness constant B meV/u.c.a. fitted to increase in band energies $E(\theta)=B(1-\cos\theta)$ due to noncollinearity of local spin moments for CMS/MgO(001) and Fe/MgO(001) junctions. 1st and 2nd indicate first and second layer at the interface with MgO, respectively. u.c.a. is unit-cell area ~32 Å^2. Ref.[81]

B meV/u.c.a.	Co^{1st}	Co^{2nd}	Mn^{1st}	Fe^{1st}
Bulk (CMS or Fe)	414	414	565	600
MgO interface	145	347	529	753

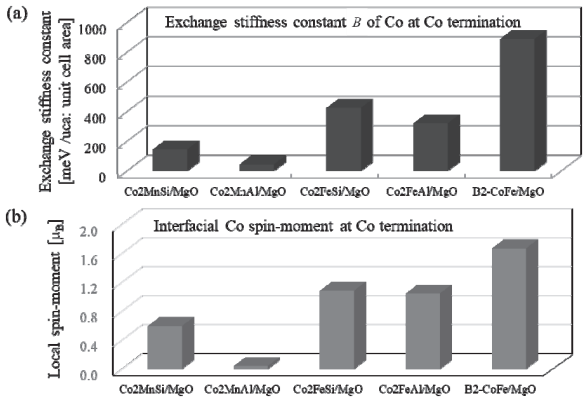

Fig. 6 (a) Exchange stiffness constant B of Co atom at Co termination of various MgO interfaces with Co-based Heusler compounds and B2-CoFe. Estimation of exchange stiffness constant B is same as in Fig. 5(a). (b) Interfacial Co spin moments at Co terminations of various MgO interfaces with Co-based Heusler compounds and B2-CoFe.

magnetic excitation modes at interfacial regions by a single excitation mode of interfacial spin moments given by the in-plane unit cell $E(\theta)$. If other magnon excitation modes are considered, the temperature dependence of TMR shown in Fig. 5(b) will change. However, the inclusion of the other excitation modes in equation (2) will lead to a further decrease in the TMR ratio at RT, and the chemical trend of the exchange stiffness at the interface has little dependence on the excitation modes. Therefore, our conclusion that the significant reduction of the TMR ratio of CMS/MgO/CMS MTJs at RT can be attributed to the interfacial spin-flip conductance does not change with a more accurate estimation of the thermally averaged tunneling conductance.

3.6 Enhancement of interface exchange stiffness

It was concluded that the reduction in the TMR ratio in CMS/MgO/CMS MTJs at RT can be attributed to spin-flip scattering in the interfacial region caused by thermal fluctuation of interfacial and sub-interfacial Co layers, and to suppress reduction in the TMR ratio at RT, it is important to enhance the exchange stiffness of Co layers at CMS/MgO junctions. Thus, I calculated the exchange stiffness constant at the interface of MgO for the other Heusler compounds and B2-CoFe. Fig. 6 shows a bar graph of the inter-atomic layer exchange stiffness constant at each interface. As shown in Fig. 6, very large exchange stiffness constants were obtained for the Co-terminated B2-CoFe/MgO interface, indicating that the B2-CoFe/MgO interface is very robust against thermal fluctuation.

Furthermore, the exchange stiffness of the Co-terminated Co_2FeSi(CFS)/MgO and Co_2FeAl(CFA)/MgO interfaces is larger than that of CMS/MgO and Co_2MnAl(CMA)/MgO interfaces. Thus, in order to suppress the thermal fluctuation at the interface with MgO, CFS and CFA are better than CMS and CMA. It was considered that the behavior of the exchange stiffness in the interfacial region is related to the behavior of the interfacial spin moments, because the exchange stiffness constant is proportional to the square of the local spin moments. In fact, as can be seen here, the behavior of the interfacial Co spin moments is consistent with the behavior of the interfacial exchange stiffness constant. This means that the enhancement of the interfacial Co spin moment is effective to obtain a large exchange stiffness constant and suppress the thermal fluctuation of Co spin moments at the MgO junction.

3.7 New physical property for temperature dependence of TMR

Recently, a new physical property characterizing the temperature dependence of TMR in MTJs was proposed in ref. [90] It was found that the intra-atomic s–d exchange coupling J_{sd} at the interface was also a key parameter in the reduction of TMR at RT. Masuda described the temperature dependent spin-flip Hamiltonian including J_{sd} at the interface Fe of Fe/MgO/Fe(001) MTJs by the coherent potential approximation of various magnetization directions according to the temperature dependence of the magnetization up to the Curie temperature. A smaller J_{sd} can disconnect the coupling between conductive s electrons and localized d electrons, leading to suppression of the spin-flip scattering at the interface. Therefore, ferromagnetic materials with smaller J_{sd} will be preferable to obtain larger TMR at RT. This new physical parameter J_{sd} will also be important for improving the large temperature dependence of the TMR of Heusler based-MTJs.

4. Spin-dependent transport in CPP-GMR devices

4.1 Valet-Fert model

According to Valet and Fert's two-current model,[91] the resistance change-area product between parallel and antiparallel magnetization configurations ($\Delta RA = R_{AP}A - R_PA$) can be expressed by two intrinsic factors in spin-dependent electron scattering. They are the bulk spin-asymmetry coefficient (β) in ferromagnetic (FM) layers and the interfacial spin-asymmetry coefficient (γ), which are included in the following equation,

$$\Delta RA = (\beta\,\rho^*_F + 2\,\gamma\,\rho^*_N\,r^*_b)/(\,\rho^*_F\,t_F + \rho^*_N\,t_N + 2\,r^*_b) \quad (3)$$

where ρ^*_F and ρ^*_N are the resistivity of the ferromagnetic electrode and the non-magnetic (NM) spacer layer in the bulk, and the t_F and t_N are the thickness of the FM and NM layers, respectively. The r^*_b is the spin-independent interface resistance. The β is enhanced by using the HMF in the FM layer, while enhancement of the γ is accomplished by reduction of the interface resistance RFM/NM through the choice of non-ferromagnetic (NM) spacers. Here, I mainly discuss the γ in HFM/NM interface, because the temperature dependence of is much larger than that of the bulk spin

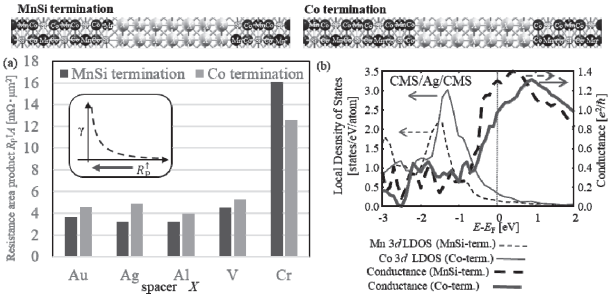

Fig. 7 (a) Bar graph comparing transmittance of CMS/*X*/CMS(001) for *X* = Au, Ag, Al, V and Cr with MnSi and Co termination. (b) LDOS of interfacial Co-*d* at Co termination and interfacial Mn-*d* at MnSi termination in CMS/Ag/CMS(001), together with transmittance averaged over the whole $\mathbf{k}_{\parallel}$ region as function of energy relative to Fermi energy. ref. [92].

asymmetry ß.

The γ is expressed by the majority-spin resistance ($R_P{}^{\uparrow}$) and minority-spin interface resistance ($R_P{}^{\downarrow}$) in the parallel magnetization configuration as follows,

$$\gamma = (R_P{}^{\downarrow} - R_P{}^{\uparrow})/(R_P{}^{\downarrow} + R_P{}^{\uparrow}) \quad (4)$$

The $R_P{}^{\downarrow}$ at the HMF/NM interface is determined by the interface state-mediated spin-flip scattering, as discussed in the previous section, because there are no states around the Fermi level of HMF minority-spin states in the bulk. In HMF/NM junctions, there are many scattering processes, making them complicated compared with HMF/insulator junctions such as Heusler/MgO. This results in a finite value for $R_P{}^{\downarrow}$ in the HMF/NM junctions, which will be difficult to control experimentally. On the other hand, the $R_P{}^{\uparrow}$ will be determined by the matching of the conductive channel between the majority-spin states of HMF and NM. Thus, in CPP-GMR devices with HMFs, matching of the majority-spin band dispersions with the NM spacer is important to reduce the $R_P{}^{\uparrow}$ of HMF/NM interfaces. As shown in the inset of Fig. 7(a), γ will rapidly increase with decreasing $R_P{}^{\uparrow}$ under fixed $R_P{}^{\downarrow}$. This means that the choice of NM spacer layer is very important to enhance the CPP-GMR with HFM Heusler compounds.

4.2 Comparison of the transmittance for CMS/*X*/CMS

As discussed in ref., [56] the transport properties obtained from the Landauer formula do not give the real conductance and resistance for a three-dimensional metallic multilayer. However, our aim in this paper is not to obtain the quantitatively correct conductance and resistance of HFM/NM/HFM junctions, but to clarify the differences in the conductance and resistance thorough HFM/NM junctions depending on the NM spacer and the interfacial termination. If the electrode region (ferromagnetic layer) consists of Co_2MnSi (CMS) for all cases, the difference in resistance between HFM/NM/HMF and HFM/NM'/HFM junctions indicates the difference in the interfacial resistance between the HFM/NM and HFM/NM' junctions, which can originate from electron scattering due to changes in the local potential and band structures at the interfacial region. Furthermore, a completely epitaxial multi-layer was assumed, where the crystal momentum parallel to the layer (or $\mathbf{k}_{\parallel}$) is conserved because of the two-dimensional periodicity of the system, and the number of conductive channels perpendicular to the plane is less than about five or six per $\mathbf{k}_{\parallel}$. Therefore, the ballistic transport calculations from the Landauer formula can be applied to evaluate the difference in the interfacial resistance depending on the band structures of the materials on both sides of the interface. This point has already been confirmed in our previous work in ref. [56] where the difference in the resistance-area products in the ballistic transport calculation between CMS/Cr/CMS(001) and CMS/Ag/CMS(001) is roughly comparable to that obtained experimentally. It is considered that this justifies the use of the Landauer formula for the investigation of the interfacial resistance of all metallic multilayers depending on the non-ferromagnetic spacer and the interfacial termination.

Figure 7 shows the majority-spin resistance-area product of CMS/*X*/CMS(001) with MnSi termination and Co termination for NM spacer *X* = fcc-Au, fcc-Ag, fcc-Al, bcc-V, and anti-ferromagnetic bcc-Cr in the parallel magnetization configuration.[92] First, Fig. 7 shows that the majority-spin resistance-area product $R_P{}^{\uparrow}A$ of the junctions with *X* = Au, Ag, Al, and V is about 3~5 mΩ·μm², which corresponds to a conductance of 0.6~1.0 G_0, where $G_0 = e^2/h$ is the ballistic conductance without scattering in the Landauer formula. On the other hand, the junctions with anti-ferromagnetic bcc-Cr spacer are about 13~16 mΩ·μm², which is 3~5 larger than that with the other spacer. These results qualitatively agree with recent experimental results on CPP-GMR devices incorporating epitaxial CMS/Ag/CMS and CMS/Cr/CMS, where a smaller resistance-area product has been obtained for the CMS/Ag(001) interface than for CMS/Cr(001).

The other feature of the transmittance of CMS/*X*/CMS(001) shown in Fig. 7 is the interface-structure dependence, i.e., the resistance-area product with Co termination is larger than that with MnSi termination except for the anti-ferromagnetic bcc-Cr spacer. Analyzing the $\mathbf{k}_{\parallel}$-dependence of the majority-spin transmittance at $E = E_F$ for CMS/*X*/CMS with Co and MnSi termination, I found that the difference in transmittance between the two terminations is significant at $k_x \neq 0$, especially for *X* = Ag, Au, Al and V. This means that the transmittance in the whole $\mathbf{k}_{\parallel}$ region contributes to the interface-structure dependence. To understand this, I show in Fig. 7(b) the local density of states (LDOS) of interfacial Co-*d* at the Co-terminated interface and interfacial Mn-3d at the MnSi-terminated interface in CMS/Ag(001), together with the transmittance averaged

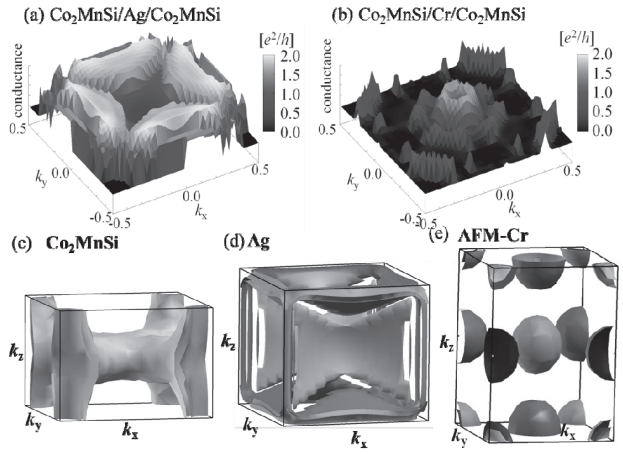

Fig. 8 Majority-spin conductance in parallel magnetization configuration calculated for (a) CMS/Ag/CMS and (b) CMS/Cr/CMS as function of $\mathbf{k}_{\parallel} = (k_x, k_y)$. Fermi surfaces in Brillouin zone corresponding to tetragonal unit cell of (c) $L2_1$-CMS, (d) fcc-Ag, and (e) anti-ferromagnetic (AFM) bcc-Cr plotted by XCRYSDEN.[93] ref.[56]

over the whole $\mathbf{k}_{\parallel}$ region as a function of the energy relative to the Fermi energy. It is evident that the transmittance increases with the decrease in the *d* component of the LDOS of interfacial atoms, indicating that the interfacial d-orbitals act as a scatterer of electrons. Furthermore, I found that the LDOS of Co-*d* at the Co termination shows large components at the Fermi level compared with those of Mn at the MnSi termination. The large *d*-components at the interfacial regions cause additional reflection of propagating electrons, leading to the large interfacial resistance in metallic multilayer. These features can be observed also in the LDOS of CMS/Au, CMS/Al and CMS/V interfaces.

4.3 Fermi surface matching at HFM/NM interface

Figures 8(a) and (b) show the $\mathbf{k}_{\parallel}$-dependence of the majority-spin conductance in the parallel magnetization configuration of CMS/Ag/CMS and CMS/Cr/CMS. It is clearly seen that the conducting channels of CMS/Cr/CMS are restricted to a small region around $\mathbf{k}_{\parallel} = (0,0)$. On the other hand, highly conducting channels spread over almost the entire region in the $\mathbf{k}_{\parallel}$ plane for CMS/Ag/CMS. The highly conducting region in the $\mathbf{k}_{\parallel}$ plane can be understood qualitatively by considering the matching of the Fermi surface over the $\mathbf{k}_{\parallel}$-plane between CMS and Ag.

Figures 8(c)-(e) show the Fermi surfaces in the Brillouin zones of $L2_1$-CMS, fcc-Ag, and AFM bcc-Cr with a tetragonal unit cell. A large overlapping area of the Fermi surface can be seen on the $\mathbf{k}_{\parallel}$-plane between CMS and Ag, resulting in the small resistance-area product ($2R_{\mathrm{CMS/Ag}}A$ = 3.21 mΩ·μm^2) for CMS/Ag/CMS, while the mismatch of the Fermi surface between CMS and Cr causes the large resistance-area product

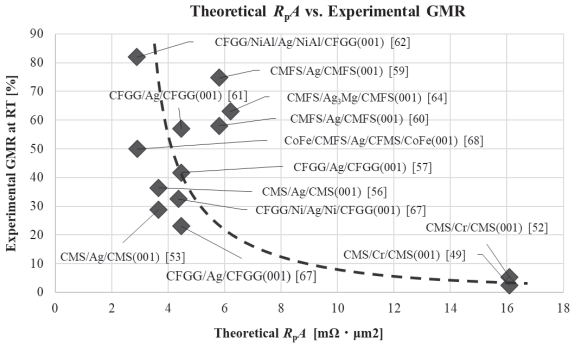

Fig. 9 Correlation between experimental CPP-GMR ratios at room temperature vs. theoretical resistance-area product R_P for various CPP-GMR devices in experiments. Broken line indicates interface spin asymmetry γ as function of majority-spin interface resistance in parallel magnetization $R_P{}^{\uparrow}$.

($2R_{\mathrm{CMS/Cr}}A$ = 16.1 mΩ·μm^2) of CMS/Cr/CMS. Although no conductance (infinite resistance) is expected in the minority-spin channel in ideal half-metals, a finite resistance-area product could appear in the minority-spin channel in real half-metals owing to such reasons such as atomic disorder, thermal fluctuation of magnetic moments, spin-orbit coupling, and so on. The minority-spin resistance-area product causes a reduction in both β and γ. Thus, one can expect a larger value of γ for CMS/Ag/CMS compared to CMS/Cr/CMS, since the majority-spin resistance-area product of CMS/Ag/CMS is much smaller than that of CMS/Cr/CMS.

Experimentally, the CMS/Ag/CMS and CMS/Cr/CMS junctions with the same annealing temperature (350°C) and exactly the same stacking structure except for the spacer layer showed *RA* of 51.4 and 66.9 mΩ·μm^2, respectively.[56] Here, the difference of *RA* (~ 15.5 mΩ·μm^2) between them is mainly caused by the difference in interface resistances, i.e., $R_{\mathrm{CMS/Ag}}A$ and $R_{\mathrm{CMS/Cr}}A$, because the contribution of the bulk resistance in Ag and Cr spacers is negligibly small. Although the experimental RA is much higher than the calculated $2R_{\mathrm{CMS/NM}}A$ (NM = Ag or Cr) since it includes all of resistances in the CPP-pillar, the difference in *RA*, i.e., $2R_{\mathrm{CMS/Cr}}A - 2R_{\mathrm{CMS/Ag}}A$ of 15.5 mΩ·μm^2 is roughly comparable to the calculated one (~ 12.9 mΩ·μm^2). This agreement is evidence of a small interface resistance and large γ between CMS and Ag due to good Fermi-surface matching, as predicted in our calculations.

4.4 Correlation between theoretical R_P and experimental CPP-GMR

Fig. 9 shows the experimental CPP-GMR in various systems as a function of the calculated majority-spin resistance-area product in parallel magnetization for the corresponding systems. As can be seen in Fig. 9, the

experimental CPP-GMR ratio increases with the decrease in the theoretical RPA, which is roughly consistent with the $R_{P}{}^{\uparrow}$ dependence of the interface spin asymmetry γ as shown in the inset of Fig. 7. This means that the enhancement of γ by the matching of the conductive channel between HFM and NM through Fermi surface matching is very important to obtain large CPP-GMR. In experiments, insertion of B2-type NiAl between $Co_2FeGa_{0.5}Ge_{0.5}$ (CFGG) and the Ag spacer dramatically enhanced the CPP-GMR and ΔRA both at LT and RT[62]. This modification was motivated by a theoretical calculation showing that the Fermi surface matching between CFGG and B2-type NiAl is much better than that of CFGG and Ag. Furthermore, the experimental results showed that not only NiAl but also Ni insertion between CFGG and the Ag spacer enhanced the CPP-GMR[67]. This result is also confirmed by theoretical calculations showing that CFGG/Ni/Ag/Ni/CFGG exhibits smaller $R_{P}{}^{\uparrow}$ than CFGG/Ag/CFGG. More recently, half-metallic $Co_2FeMnSi$ (CFMS) was inserted between A2-CoFe and Ag spacer, and the CPP-GMR was maximized when the thickness of CFMS was around 7 nm[68]. One possible reason for the large CPP-GMR was attributed to the better Fermi surface matching of CFMS/CoFe as compared with CoFe/Ag. All these results indicate that Fermi surface matching between HFM and the NM spacer layer is a key factor in enhancing the CPP-GMR for future ultra-sensitive magneto-resistive sensors.

5. Summary

In this paper, first-principles studies on electronic structures and ballistic transport properties of HMF Co-based Heusler compound-based magneto-resistive devices were reviewed.

The effects of spin-flip scattering by interfacial noncollinear magnetic structures on the TMR ratios of MTJs with Co_2MnSi(CMS) and MgO were investigated using first-principles calculations. It was found that the effects of the noncollinearity of interfacial Co spin moments on the TMR are significant in determining the spin-flip conductance. Furthermore, the inter-atomic layer exchange stiffness constant of interfacial and sub-interfacial Co spin moments at CMS/MgO junctions is much smaller than that in bulk regions. From these results, I conclude that the low TMR ratio at room temperature in MTJs with half-metallic Co-based full Heusler compounds can be attributed to spin-flip scattering by the noncollinear magnetic structures of interfacial Co as a result of thermal fluctuations. These results are validated by recent experimental results, i.e., the significant reduction in the TMR ratios of CMS/MgO/CMS MTJs at RT compared to those of Fe/MgO/Fe MTJs. This means that the spin-flip scattering at the interface is at least as important as any other effect. I showed that the interfacial exchange stiffness can be strongly enhanced by inserting an ultrathin B2-CoFe layer in CMS/MgO junctions, leading to a larger TMR ratio at room temperature.

For CPP-GMR, the ballistic conductance of HFM/NM/HFM was calculated in order to clarify the origin of interfacial resistance. The majority-spin transmittance of CMS/*X*/CMS(001) in the parallel magnetization configuration was calculated by the Landauer formula, and it was found that the matching of the Fermi surface projected to the two-dimensional Brillouin zone in in-plane wave vector $\mathbf{k}_{\parallel}$ between CMS and NM spacers is a main contributing factor to the interfacial resistance among spacers. The experimental CPP-GMR was well reproduced as a function of the theoretical resistance-area product in parallel magnetization through the equation of interface spin asymmetry γ.

All these findings suggest that the TMR ratios of MTJs and CPP-GMR with half-metallic Co-based full Heusler compounds can be designed by controlling their interfaces, which is worth further investigation.

Acknowledgements I am grateful to M. Shirai and K. Abe of Tohoku University, K. Hono, S. Mitani, Y. Sakuraba, H. Sukegawa, S. Kasai, K. Masuda and I. Kurniawan of the Na-tional Institute for Materials Science, and K. Nawa of Mie University for valuable discussions on this work. This work was partly supported by Grants-in-Aid for Scientific Research (Grant Nos. 17H06152, 20H00299, 20H02190, 20H02186, 21H01750 and 22H04966) from the Japan Society for the Pro-motion of Science, Center for Spintronics Research Network (CSRN) of Osaka University, and the Cooperative Research Project Program of the Research Institute of Electrical Communication in Tohoku University.

References

1) M. N. Baibich, J. M. Broto, A. Fert, F. Nguyen Van Dau, F. Petroff, P. Etienne, G. Creuzet, A. Friederich, and J. Chazelas: *Phys. Rev. Lett.* **61**, 2472 (1988).
2) G. Binasch, P. Grünberg, F. Saurenbach, and W. Zinn: *Phys. Rev. B* **39**, 4828 (1989).
3) T. Miyazaki and N. Tezuka: *J. Magn. Magn. Mater.* **139**, L231 (1995).
4) T. Hanyu, T. Endoh, D. Suzuki, H. Koike, Y. Ma, N. Onizawa, M. Natsui, S. Ikeda, and H. Ohno: *Proc. IEEE* **104**, 1844 (2016).
5) D. Ielmini and S. Ambrogio: *Nanotechnology* **31**, 092001 (2020).
6) S. Yuasa, T. Nagahama, A. Fukushima, Y. Suzuki, and K. Ando: *Nature Material* **3**, 868 (2004).
7) S. S. P. Parkin, C. Kaiser, A. Panchula, P. M. Rice, B. Hughes, M. Samant, and S.-H. Yang: *Nature Material* **3**, 862 (2004).
8) S. Ikeda, J. Hayakawa, Y. M. Lee, F. Matsukura, Y. Ohno, T. Hanyu, and H. Ohno: *IEEE Trans. Electron Dev.* **54**, 991 (2007).
9) W. H. Butler, X.-G. Zhang, T. C. Schulthess, and J. M. MacLaren: *Phys. Rev. B* **63**, 054416 (2001).
10) J. Mathon and A. Umerski: *Phys. Rev. B* **63**, 220403(R) (2001).
11) R. A. de Groot, F. M. Mueller, P. G. van Engen, and K. H. J. Buschow: *Phys. Rev. Lett.* **50**, 2024 (1983).
12) K. Schwarz: *J. Phys. F* **16**, L211 (1986).

13) W. E. Pickett and D. J. Singh: *Phys. Rev. B* **53**, 1146 (1996).
14) S. Ishida, S. Fujii, S. Kashiwagi, and S. Asano: *J. Phys. Soc. Jpn* **64**, 2152 (1995).
15) S. Picozzi, A. Continenza, and A. J. Freeman: *Phys. Rev. B* **66**, 094421 (2002).
16) I. Galanakis, P. H. Dederichs, and N. Papanikolaou: *Phys. Rev. B* **66**, 174429 (2002).
17) Y. Miura, K. Nagao, and M. Shirai: *Phys. Rev. B* **69**, 144413 (2004); *J. Appl. Phys.* **95**, 7225 (2004).
18) S. Picozzi, A. Continenza and A. J. Freeman: *Phys. Rev. B* **69**, 094423 (2004).
19) Y. Miura, M. Shirai, and K. Nagao: *J. Appl. Phys.* **99**, 08J112 (2006).
20) M. Miyamoto, A. Kimura, Y. Miura, M. Shirai, M. Ye, Y. Cui, K. Shimada, H. Namatame, M. Taniguchi, Y. Takeda, Y. Saitoh, E. Ikenaga, S. Ueda, K. Kobayashi and T. Kanomata: *Phys. Rev. B* **79**, 100405(R) (2009).
21) S. Ueda, Y. Miura, Y. Fujita and Y. Sakuraba: *Phys. Rev. B* **106**, 075101 (2022).
22) B. L. Gyorffy, A. J. Pindor, J. Staunton, G. M. Stocks and H. Winter: *J. Phys. F Met. Phys.* **15**, 1337 (1985).
23) K. Nawa, I. Kurniawan, K. Masuda, Y. Miura, C. E. Patrick and J. B. Staunton: *Phys. Rev. B* **102**, 054424 (2020).
24) I. Kurniawan, K. Nawa, K. Masuda, Y. Miura and K. Hono: *Acta Materialia* **218**, 117218 (2021).
25) I. Kurniawan, Y. Miura and K. Hono: *Phys. Rev. Mat.* **6**, L091402 (2022).
26) K. Inomata, S. Okamura, R. Goto, and N. Tezuka: *Jpn. J. Appl. Phys.* **42**, L419 (2003).
27) H. Kubota, J. Nakata, M. Oogane, Y. Ando, A. Sakuma, and T. Miyazaki: *Jpn. J. Appl. Phys.* **43**, L984 (2004).
28) S. Okamura, A. Miyazaki, S. Sugimoto, N. Tezuka, and K. Inomata: *Appl. Phys. Lett.* **86**, 232503 (2005).
29) Y. Sakuraba, M. Hattori, M. Oogane, Y. Ando, H. Kato, A. Sakuma, T. Miyazaki and H. Kubota: *Appl. Phys. Lett.* **88**, 192508 (2006).
30) N. Tezuka, N. Ikeda, A. Miyazaki, S. Sugimoto, M. Kikuchi and K. Inomata: *Appl. Phys. Lett.* **89**, 112514 (2006).
31) T. Marukame and M. Yamamoto: *Appl. Phys. Lett.* **101**, 083906 (2007).
32) S. Tsunegi, Y. Sakuraba, M. Oogane, K. Takanashi and Y. Ando: *Appl. Phys. Lett.* **93**, 112506 (2008).
33) T. Ishikawa, N. Itabashi, T. Taira, K-i. Matsuda, T. Uemura and M. Yamamoto: *Appl. Phys. Lett.* **94**, 092503 (2009).
34) N. Tezuka, N. Ikeda, F. Mitsuhashi and S. Sugimoto: *Appl. Phys. Lett.* **94**, 162504 (2009).
35) H. Sukegawa, W. Wang, R. Shan, T. Nakatani, K. Inomata and K. Hono: *Phys. Rev. B* **79**, 184418 (2009).
36) W. Wang, H. Sukegawa, K. Inomata: *Phys. Rev. B* **82**, 092402 (2010).
37) H. Liu, Y. Honda, T. Taira, K.-i. Matsuda, M. Arita, T. Uemura and M. Yamamoto: *Appl. Phys. Lett.* **101**, 132418 (2012).
38) H. Liu, T. Kawami, K. Moges, T. Uemura, M. Yamamoto, F. Shi and P. M. Voyles: *J. Phys. D: Appl. Phys.* **48**, 164001 (2015).
39) T. Scheike, H. Sukegawa, K. Inomata, T. Ohkubo, K. Hono and S. Mitani: *Appl. Phys. Exp.* **9**, 053004 (2016).
40) B. Hu, K. Moges, Y. Honda, H. Liu, T. Umemura and M. Yamamoto: *Phys. Rev. B* **94**, 094428 (2016).
41) S. Kasai, Y. K. Takahashi, P.-H. Cheng, Ikhtar, T. Ohkubo, K. Kondou, Y. Otani, S. Mitani and K. Hono: *Appl. Phys. Lett.* **109**, 032409 (2016).
42) K. Mukaiyama, J. W. Jung, H. Sepehri-Amin, S. Kasai, T. Furubayashi, T. Ohkubo and K. Hono: *Appl. Phys. Lett.* **114**, 172402 (2019).
43) T. Scheike, Z. Wen, H. Sukegawa and S. Mitani: *Appl. Phys. Lett.* **122**, 112404 (2023).
44) T. Kubota, Y. Miura, D. Watanabe, S. Mizukami, F. Wu, H. Naganuma, X. Zhang, M. Oogane, M. Shirai, Y. Ando and T. Miyazaki: *Appl. Phys. Exp.* **44**, 043002 (2011).
45) H. Kurt, N. Baadji, K. Rode, M. Venkatesan, P. Stamenov, S. Sanvito and J. M. D. Coey: *Appl. Phys. Lett.* **101**, 132410 (2012).
46) W. S. Yun, G.-B. Cha, I. G. Kim, S. H. Rhim and S. C. Hong: *J. Phys.: Condens. Matter* **24**, 416003 (2012).
47) Y. Miura and M. Shirai: *IEEE Trans. Mag.* **50**, 1400504 (2014).
48) T. Kubota, S. Mizukami, Q. L. Ma, H. Naganuma, M. Oogane, Y. Ando and T. Miyazaki: *J. Appl. Phys.* **115**, 17C704 (2014).
49) K. Yakushiji, K. Saito, S. Mitani, and K. Takanashi, Y. K. Takahashi, and K. Hono: *Appl. Phys. Lett.* **88**, 222504 (2006).
50) T. Mizuno, Y. Tsuchiya, T. Machita, S. Hara, D. Miyauchi, K. Shimazawa, T. Chou, K. Noguchi, and K. Tagami: *IEEE Trans. Magn.* **44**, 3584 (2008).
51) T. Furubayashi, K. Komada, T. Furubayashi, H. Sukegawa, Y. K. Takahashi, K. Inomata, and K. Hono: *Appl Phys. Lett.* **93**, 122507 (2008).
52) Y. Sakuraba, T. Iwase, K. Sato, S. Mitani and K. Takahashi: *Appl. Phys. Lett.* **94**, 012511 (2009).
53) T. Iwase, Y. Sakuraba, S. Bosu, K. Saito, S. Mitani, and K. Takanashi: *Appl. Phys. Exp.* **2**, 063003 (2009).
54) T. M. Nakatani, T. Furubayashi, S. Kasai, H. Sukegawa, Y. K. Takahashi, S. Mitani and K. Hono: *Appl. Phys. Lett.* **99**, 182505 (2011).
55) N. Hase, B. S. D. Ch. S. Varaprasad, T. M. Nakatani, H. Sukegawa, S. Kasai, Y. K. Takahashi, T. Furubayashi and K. Hono: *J. Appl. Phys.* **108**, 093916 (2010).
56) Y. Sakuraba, K. Izumi, T. Iwase, S. Bosu, K. Saito, K. Takanashi, Y. Miura, K. Futatsukawa, K. Abe, and M. Shirai: *Phys. Rev. B* **82**, 094444 (2010).
57) Y. K. Takahashi, A. Srinivasan, B. Varaprasad, A. Rajanikanth, N. Hase, T. M. Nakatani, S. Kasai, T. Furubayashi, and K. Hono: *Appl. Phys. Lett.* **98**, 152501 (2011).
58) M. J. Carey, S. Maat, S. Chandrashekariaih, J. A. Katine, W. Chen, B. York, and J. R. Childress: *J. Appl. Phys.* **109**, 093912 (2011).
59) J. Sato, M. Oogane, H. Naganuma and Y. Ando: *Appl. Phys. Exp.* **4**, 113005 (2011).
60) Y. Sakuraba, M. Ueda, Y. Miura, K. Sato, S. Bosu, K. Saito, M. Shirai, T. J. Konno and K. Takanashi: *Appl. Phys. Lett.* **101**, 252408 (2012).
61) S. Li, Y. K. Takahashi, T. Furubayashi and K. Hono: *Appl. Phys. Lett.* **103**, 042405 (2013).
62) J. W. Jung, Y. Sakuraba, T. T. Sasaki, Y. Miura and K. Hono: *Appl. Phys. Lett.* **108**, 102408 (2016).
63) M. Inoue, B. Hu, K. Moges, K. Inubushi, K. Nakada, M. Yamamoto and T. Uemura: *Appl. Phys. Lett.* **111**, 082403 (2017).
64) T. Kubota, Y. Ina, Z. Wen, H. Narisawa and K. Takanashi: *Phys. Rev. Mat.* **1**, 044402 (2017).
65) S. Li, T. Nakatani, K. Masuda, Y. Sakuraba, X. D. Xu, T. T. Sasaki, H. Tajiri, Y. Miura, T. Furubayashi and K. Hono: *Acta Materialia* **142**, 49 (2018).
66) T. Kubota, Y. Ina, Z. Wen and K. Takanashi: *J. Mag. Mag. Mat.* **474**, 365 (2019).
67) B. Büker, J. W. Jung, T. Sasaki, Y. Sakuraba, Y. Miura, T. Nakatani, A. Hütten and K. Hono: *Phys. Rev. B* **103**, L140405 (2021).
68) Y. Fujita, Y. Miura, T. Sasaki, T. Nakatani, K. Hono and Y. Sakuraba: *Phys. Rev. B* **104**, L140403 (2021).
69) J. P. Perdew, K. Burke, and M. Ernzerhof: *Phy. Rev. Lett.* **77**, 3865 (1996).
70) P. Giannozzi, S. Baroni, N. Bonini, M. Calandra, R. Car, C. Cavazzoni, D. Ceresoli, G. L. Chiarotti, M. Cococcioni, I. Dabo, A. Dal Corso, S. Fabris, G. Fratesi, S. de Gironcoli, R.

Gebauer, U. Gerstmann, C. Gougoussis, A. Kokalj, M. Lazzeri, L. Martin-Samos, N. Marzari, F. Mauri, R. Mazzarello, S. Paolini, A. Pasquarello, L. Paulatto, C. Sbraccia, S. Scandolo, G. Sclauzero, A. P. Seitsonen, A. Smogunov, P. Umari, R. M. Wentzcovitch: *J. Phys.: Condens. Matter* **21**, 395502 (2009).
71) R. Landauer: *Philos. Mag.* **21**, 863 (1970).
72) H. J. Choi and J. Ihm: *Phys. Rev. B* **59**, 2267 (1999).
73) A. Smogunov, A. Dal Corso, and E. Tosatti: *Phys. Rev. B* **70**, 045417 (2004).
74) Y. Miura, H. Uchida, Y. Oba, K. Abe and M. Shirai: *Phys. Rev. B* **78**, 064416 (2008).
75) Y. Miura, H. Uchida, Y. Oba, K. Nagao and M. Shirai: *J. Phys.: Condens. Matter* **19**, 365228 (2007).
76) P. Mavropoulos, M. Lezaic, and S. Blügel: *Phys. Rev. B* **72**, 174428 (2005).
77) M. Lezaic, P. Mavropoulos, J. Enkovaara, G. Bihlmayer and S. Blügel: *Phys. Rev. Lett.* **97**, 026404 (2006).
78) L. Chioncel, Y. Sakuraba, E. Arrigoni, M. I. Katsnelson, M. Oogane, Y. Ando, T. Miyazaki, E. Burzo, and A. I. Lichtenstein: *Phys. Rev. Lett.* **100**, 086402 (2008).
79) J. Kübler, K-H. Höck, J. Sticht and A. R.Williams: *J. Phys. F: Met. Phys.* **18**, 469 (1988).
80) K. Nakamura, T. Ito, A. J. Freeman, L. Zhong and J. Fernandez-de-Castro: *Phys. Rev. B* **67**, 014420 (2003).
81) Y. Miura, K. Abe and M. Shirai: *Phys. Rev. B* **83**, 214411 (2011).
82) J. Kübler, G. H. Fecher and C. Felser: *Phys. Rev B* **76**, 024414 (2007).
83) J. Kübler, A. R. Williams and C. B. Sommers: *Phys. Rev. B* **28**, 1745 (1983).
84) T. Saito, T. Katayama, T. Ishikawa, M. Yamamoto, D. Asakura, T. Koide, Y. Miura and M. Shirai: *Phys. Rev. B* **81**, 144417 (2010).
85) L. M. Sandratskii: *Phys. Rev. B* **78**, 094425 (2008).
86) M. Weinert, R. E. Watson and J. W. Davenport: *Phys. Rev. B* **32**, 2115 (1985).
87) G. H. O. Daalderop, P. J. Kelly and M. F. Schuurmans: *Phys. Rev. B* **41**, 11919 (1990).
88) S. Lounis and P. Dederichs: *Phys. Rev. B* **82**, 180404(R) (2010).
89) A. Sakuma, Y. Toga, and H. Tsuchiura: *J. Appl. Phys.* **105**, 07C910 (2009).
90) K. Masuda, T. Tadano and Y. Miura: *Phys. Rev. B* **104**, L180403 (2021).
91) T. Valet and A. Fert: *Phys. Rev. B* **48**, 7099 (1993).
92) Y. Miura, K. Futatsukawa, S. Nakajima, K. Abe and M. Shirai: *Phys. Rev. B* **84**, 134432 (2011).
93) A. Kokalj: *Comput. Mater. Sci.* **28**, 155 (2003).

Received Mar. 31, 2023; Accepted Apr. 19, 2023